Eur. Phys. J. B (2018) 91: 12
https://doi.org/10.1140/epjb/e2017-80465-0

THE EUROPEAN PHYSICAL JOURNAL B

Regular Article

Tunneling conductance oscillations in spin–orbit coupled metal–insulator–superconductor junctions

Priyadarshini Kapri[a] and Saurabh Basu

Department of Physics, Indian Institute of Technology Guwahati, Guwahati, Assam 781039, India

Received 8 August 2017 / Received in final form 30 October 2017
Published online 17 January 2018 –

Abstract. The tunneling conductance for a device consisting of a metal–insulator–superconductor (MIS) junction is studied in presence of Rashba spin–orbit coupling (RSOC) via an extended Blonder–Tinkham–Klapwijk formalism. We find that the tunneling conductance as a function of an effective barrier potential that defines the insulating layer and lies intermediate to the metallic and superconducting electrodes, displays an oscillatory behavior. The tunneling conductance shows high sensitivity to the RSOC for certain ranges of this potential, while it is insensitive to the RSOC for others. Additionally, when the period of oscillations is an odd multiple of a certain value of the effective potential, the conductance spectrum as a function of the biasing energy demonstrates a contrasting trend with RSOC, compared to when it is not an odd multiple. The explanations for the observation can be found in terms of a competition between the normal and Andreev reflections. Similar oscillatory behavior of the conductance spectrum is also seen for other superconducting pairing symmetries, thereby emphasizing that the insulating layer plays a decisive role in the conductance oscillations of a MIS junction. For a tunable Rashba coupling, the current flowing through the junction can be controlled with precision.

1 Introduction

Charge transport through metal–insulator–superconductor (MIS) junctions has been a subject of considerable interest both theoretically and experimentally owing to the fundamental physics embedded therein and the possibility of fabricating devices at very small length scales. Tunneling spectroscopy is a direct and most effective tool to acquire information on the interparticle interaction and the nature of the superconducting gap [1,2]. When an electron incidents from the normal metal in a metal–superconductor junction with an energy lower than the superconducting gap, a cooper pair is injected into the superconducting layer, a phenomenon known as Andreev reflection (AR) [3–5]. AR is caused by the conversion of current in the normal region to a supercurrent in the superconducting region at the metal–superconductor junction.

With the advent of spintronics in the recent past, spin dependent transport through the junctions is an important subject, which has recently gained eminence because of the prospects of fabricating novel devices that are capable of manipulating the spin in addition to the charge degree of freedom [6–8]. The phenomenon of spin–orbit coupling (SOC) is key to the success of this emerging field.

In low dimensions, particularly, in the context of two dimensional electron gases (2DEG), due to breaking of reflection symmetry near the interface, such as InAs, etc. [9], the quasiparticles experience a special type of SOC, namely, Rashba spin–orbit coupling (RSOC) [10] even if both the normal and superconducting materials have bulk inversion symmetry. Thus the effect of RSOC becomes salient and hence can not be skipped. The feasibility of being able to tune the strength of RSOC using an external field [11] provides an additional impetus. Among the recent works in this field, many investigations have been carried out to study the influence of RSOC on transport properties of a 2DEG [12–25].

The Blonder–Tinkham–Klapwijk (BTK) theory [26] provides a simple interpretation of the AR by modeling the metal–superconductor interface via a δ-function type of potential or an insulating barrier of arbitrary strength and width. We use a BTK formalism to compute and perform the analysis of the conductance profile of a MIS junction in the presence of RSOC present at the interfaces separating the metal–insulator and the insulator–superconductor where the quasiparticles in the superconducting sample are described by the Bogoliubov-de Gennes (BdG) equations [27]. We are especially concerned about scrutinizing an interplay of RSOC with a number of useful parameters that characterize the MIS junction, such as the effective barrier potential of the insulating region and the different superconducting gap symmetries of the superconducting lead. The interplay of these parameters renormalize the features of the conductance spectrum in an interesting fashion and form the focus of this paper here.

[a] e-mail: priyadarshini@iitg.ernet.in

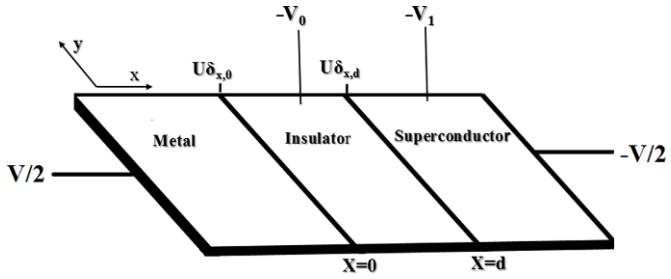

Fig. 1. Schematic illustration of the MIS junction setup.

The paper is organized as follows. In Section 2, we provide a brief discussion of BTK formalism and establish the notations which are used throughout the paper. The numerical results and their corresponding discussions of the tunneling conductance spectrum for a s-wave superconductor are discussed in Section 3.1 and the same for d and p-wave superconductor are in Section 3.2. Finally, we briefly summarize our results in Section 4.

2 Theoretical model

We consider a two dimensional MIS junction setup as shown in Figure 1 where the normal region and superconducting region occupy $x \leq 0$ and $x \geq d$ respectively with the insulating region extending from $x = 0$ to d. The $x \leq 0$ (metallic electrode) and $x \geq d$ (superconducting electrode) regions denote the electrodes that carry the current through the junctions. The interfaces of this MIS junctions are located at $x = 0$ and $x = d$. We have considered the presence of RSOC only at the interfaces of the system as interfaces denote the regions where space inversion symmetry is violated and is described by the following potential,

$$U_\sigma(x) = U\hat{n} \cdot (\hat{\sigma} \times \hat{k})\delta_{x,0} + U\hat{n} \cdot (\hat{\sigma} \times \hat{k})\delta_{x,d}. \quad (1)$$

Here we have chosen, $\hat{n} = \hat{x}$ as the unit vector along the interface normal, U is the strength of the RSOC, $\hat{\sigma}$ are the Pauli matrices, and the propagation direction is denoted by, $\hat{k}$ ($-i\nabla$ with $\hbar = 1$).

The BdG equations [27] are used here to describe the quasiparticles in the superconducting regime. The quasiparticle wave function has four components because of the extra spin degrees of freedom caused by the presence of the Rashba term. By considering a two dimensional geometry, the BdG equations can be decoupled into 2 two component equations, one for each spin, σ, as follows,

$$H_\sigma \Psi(r) = E\Psi(r) \quad (2)$$

where $\sigma = \pm 1$ denote two different spin orientations. H_σ is written as,

$$H_\sigma = \begin{pmatrix} -\frac{\nabla^2}{2} - E_F(x) + U_\sigma(x) & \tilde{\Delta} \\ \tilde{\Delta}^\dagger & \frac{\nabla^2}{2} + E_F(x) - U_\sigma(x) \end{pmatrix} \quad (3)$$

where the mass of electrons is taken as unity. The Rashba term can explicitly be written as,

$$U_\sigma(x) = -\sigma U k_F^N \sin\theta_{N1}\delta_{x,0} - \sigma U k_F^I \sin\theta_{I1}\delta_{x,d} \quad (4)$$

implying that it exists only at the junctions at $x = 0$ and $x = d$. The Fermi energy $E_F(x)$ is defined by,

$$E_F(x) = E_F^N\Theta(-x) + (E_F^N + V_0)\Theta(d - x) + (E_F^N + V_1)\Theta(x - d). \quad (5)$$

E_F^N, $(E_F^N + V_0)$ and $(E_F^N + V_1)$ are the Fermi energies of metallic, insulating and superconducting regions respectively where V_0 is the potential across the insulating barrier region and V_1 is electrostatic potential in the superconducting region which is used to tune the Fermi wavevector mismatch between the metal and superconducting region. The off-diagonal terms of the matrix are the superconducting gap parameter, $\tilde{\Delta}$. The superconducting order parameter for s-wave is a constant and given by,

$$\tilde{\Delta}_s = \Delta_0\Theta(x - d) \quad (6)$$

and the corresponding quantities for p-wave and d-wave superconductors are respectively given by [23–25,28,29],

$$\tilde{\Delta}_p = \Delta(k_\pm)\Theta(x - d) = \pm\Delta_0 e^{\pm i\theta_{S1,S2}}\Theta(x - d) \quad (7)$$

and

$$\tilde{\Delta}_d = \Delta(k_\pm)\Theta(x - d) = \Delta_0 \cos(2\theta_{S1,2} \mp 2\alpha)\Theta(x - d) \quad (8)$$

where α is the angle between the crystalline orientation and x axis (see Fig. 1c in Ref. [30]). The plus and minus signs in the gap functions are for electron and hole-like quasiparticles. The momentum (k) dependence in the $\tilde{\Delta}_{d,p}$ enters through θ_{S1} and θ_{S2} (see Eq. (12)) and $\tilde{\Delta}$ has the dimension of energy. It can be noted that the superconducting order parameters are different for electron-like and hole-like quasiparticles owing to the different phases involved between them.

Suppose an electron from the left metallic lead is injected with the excitation energy $E \geq 0$, spin σ, and incident angle θ_{N1}. The incident electron experiences the following processes, (i) AR with angle θ_{N2}, (ii) normal reflection (NR) with angle θ_{N1}, (iii) transmission as electron with angle θ_{I1} and as hole with angle θ_{I2} to insulating region, (iv) reflection as electron with angle θ_{I1} and as hole with angle θ_{I2} at the insulating and the superconducting interfaces and (v) transmission as electron like quasiparticle with angle θ_{S1} and as hole like quasiparticle with angle θ_{S2}.

The momenta of electrons and holes in the normal region are given by [30],

$$k_{N1} = k_F^N + \frac{E}{v_F^N}$$
$$k_{N2} = k_F^N - \frac{E}{v_F^N}. \quad (9)$$

Similarly, the momenta of electrons and holes in the insulating region are given by,

$$k_{I1} = k_F^I + \frac{E}{v_F^I}$$
$$k_{I2} = k_F^I - \frac{E}{v_F^I}. \tag{10}$$

Further the momenta of the electron-like and hole-like quasiparticles in superconducting region are given by,

$$q_{S1} = q_F^S + \frac{\sqrt{E^2 - \tilde{\Delta_+}^2}}{v_F^S}$$
$$q_{S2} = q_F^S - \frac{\sqrt{E^2 - \tilde{\Delta_-}^2}}{v_F^S} \tag{11}$$

where v_F^N, v_F^I and v_F^S are Fermi velocities for respective regions, ensuring different Fermi vectors in these three regions. Here we consider a simplification by setting $q_{S1} = q_{S2} = q_F^S$. This simplification introduces an error of the order $\delta q_F^S/q_F^S = \sqrt{E^2 - \tilde{\Delta}^2}/E_F^S$. The error due to this is of the order of $\tilde{\Delta}/E_F^S$. Since $\tilde{\Delta}$ is much smaller than E_F^S, this is a reasonable assumption. However we retain different symbols for them for the sake of convenience. The momentum parallel to the interface is conserved in the tunneling process. So we can write,

$$\begin{aligned} k_{N1}\sin\theta_{N1} &= k_{N2}\sin\theta_{N2} = k_{I1}\sin\theta_{I1} = k_{I2}\sin\theta_{I2} \\ &= q_{S1}\sin\theta_{S1} = q_{S2}\sin\theta_{S2}. \end{aligned} \tag{12}$$

The solutions of equation (2) in metal, insulator and superconducting regions are,

$$\begin{aligned} \Psi_N(x) = &\begin{pmatrix}1\\0\end{pmatrix} e^{ik_{N1}\cos\theta_{N1}x} + a_\sigma \begin{pmatrix}0\\1\end{pmatrix} e^{ik_{N2}\cos\theta_{N2}x} \\ &+ b_\sigma \begin{pmatrix}1\\0\end{pmatrix} e^{-ik_{N1}\cos\theta_{N1}x} \end{aligned} \tag{13}$$

$$\begin{aligned} \Psi_I(x) = &\alpha_\sigma \begin{pmatrix}1\\0\end{pmatrix} e^{ik_{I1}\cos\theta_{I1}x} + \beta_\sigma \begin{pmatrix}1\\0\end{pmatrix} e^{-ik_{I1}\cos\theta_{I1}x} \\ &+ \alpha'_\sigma \begin{pmatrix}0\\1\end{pmatrix} e^{-ik_{I2}\cos\theta_{I2}x} + \beta'_\sigma \begin{pmatrix}0\\1\end{pmatrix} e^{ik_{I2}\cos\theta_{I2}x} \end{aligned} \tag{14}$$

and

$$\begin{aligned} \Psi_S(x) = &c_\sigma \begin{pmatrix}u_+ e^{i\phi_+}\\ v_+\end{pmatrix} e^{iq_{S1}\cos\theta_{S1}x} \\ &+ d_\sigma \begin{pmatrix}v_- e^{i\phi_-}\\ u_-\end{pmatrix} e^{-iq_{S2}\cos\theta_{S2}x} \end{aligned} \tag{15}$$

respectively. Here a_σ and b_σ denote the amplitudes of reflection of hole (AR) and NR respectively in the metallic region. α_σ and β_σ denote the amplitudes of incoming and reflected electron in the insulating region where α'_σ and β'_σ are for amplitudes of incoming and reflected hole in the insulating region. Also c_σ and d_σ correspond to coefficients of transmission to the superconducting leads as electron-like quasiparticles and as hole-like quasiparticles with,

$$u_\pm = \frac{1}{\sqrt{2}}\sqrt{1 + \frac{\Omega_\pm}{E}}$$
$$v_\pm = \frac{1}{\sqrt{2}}\sqrt{1 - \frac{\Omega_\pm}{E}} \tag{16}$$

where,

$$\Omega_\pm = \sqrt{E^2 - \tilde{\Delta}_\pm^2}. \tag{17}$$

The wave functions must satisfy the boundary conditions,

$$\begin{aligned} \Psi_N(x=0) &= \Psi_I(x=0) \\ \Psi_I(x=d) &= \Psi_S(x=d) \\ \frac{d\Psi_I}{dx}(x=0) - \frac{d\Psi_N}{dx}(x=0) &= -2\sigma U k_F^N \sin\theta_{N1}\Psi_N(x=0) \\ \frac{d\Psi_S}{dx}(x=d) - \frac{d\Psi_I}{dx}(x=d) &= -2\sigma U k_F^I \sin\theta_{I1}\Psi_I(x=d). \end{aligned} \tag{18}$$

All the reflection and transmission amplitudes can be found from the boundary conditions.

In particular, the reflection amplitudes, needed to compute the conductance (see Eq. (26)), are given by,

$$\begin{aligned} a_\sigma &= \alpha'_\sigma + \beta'_\sigma \\ b_\sigma &= \alpha_\sigma + \beta_\sigma - 1 \end{aligned} \tag{19}$$

where,

$$\begin{aligned} \alpha_\sigma &= P_1 c_\sigma u_+ e^{i\phi_+} + P_2 d_\sigma v_- e^{i\phi_-} \\ \beta_\sigma &= P_3 c_\sigma u_+ e^{i\phi_+} + P_4 d_\sigma v_- e^{i\phi_-} \\ \beta'_\sigma &= P_5 c_\sigma v_+ + P_6 d_\sigma u_- \\ \alpha'_\sigma &= P_7 c_\sigma v_+ + P_8 d_\sigma u_-. \end{aligned} \tag{20}$$

The P_i's appearing above are respectively denoted by,

$$\begin{aligned} P_1 &= e^{i(X_{S1}-X_{I1})d}\left[\frac{iX_{I1} + iX_{S1} - U_{IS}}{2iX_{I1}}\right] \\ P_2 &= e^{-i(X_{S1}+X_{I1})d}\left[\frac{iX_{I1} - iX_{S1} - U_{IS}}{2iX_{I1}}\right] \\ P_3 &= (e^{i(X_{S1}-X_{I1})d} - P_1)e^{2iX_{I1}d} \\ P_4 &= (e^{-i(X_{S1}+X_{I1})d} - P_2)e^{2iX_{I1}d} \\ P_5 &= e^{i(X_{S1}-X_{I2})d}\left[\frac{iX_{I2} + iX_{S1} - U_{IS}}{2iX_{I2}}\right] \\ P_6 &= e^{-i(X_{S1}+X_{I2})d}\left[\frac{iX_{I2} - iX_{S1} - U_{IS}}{2iX_{I2}}\right] \\ P_7 &= (e^{i(X_{S1}-X_{I2})d} - P_5)e^{2iX_{I2}d} \\ P_8 &= (e^{-i(X_{S1}+X_{I2})d} - P_6)e^{2iX_{I2}d}. \end{aligned} \tag{21}$$

Further,

$$\begin{aligned} c_\sigma &= -d\frac{u_-}{v_+}\frac{L_4}{L_3} \\ d_\sigma &= \frac{1+\frac{U_{NI}+iX_{N1}}{iX_{N1}-U_{NI}}}{v_- L_2 e^{i\phi_-} - \frac{u_+u_-}{v_+}\frac{L_1L_4}{L_3}e^{i\phi^+}} \\ e^{i\phi_\pm} &= \tilde{\Delta_\pm}/|\tilde{\Delta_\pm}| \\ U_{NI} &= -2\sigma U k_{FN}\sin\theta_{N1}. \end{aligned} \tag{22}$$

All the L_i and the X_i appearing in equations (21) and (22) are given by,

$$\begin{aligned} L_1 &= P_1 + P_3 + \frac{iX_{I1}(P_1-P_3)}{iX_{N1}-U_{NI}} \\ L_2 &= P_2 + P_4 + \frac{iX_{I1}(P_2-P_4)}{iX_{N1}-U_{NI}} \\ L_3 &= P_5 + P_7 - \frac{iX_{I2}(P_5-P_7)}{iX_{N2}+U_{NI}} \\ L_4 &= P_6 + P_8 - \frac{iX_{I2}(P_6-P_8)}{iX_{N2}+U_{NI}} \\ X_{N1,N2} &= k_{N1,N2}\cos\theta_{N1,N2} \\ X_{I1,I2} &= k_{I1,I2}\cos\theta_{I1,I2} \\ X_{S1,S2} &= q_{S1,S2}\cos\theta_{S1,S2} \\ U_{IS} &= -2\sigma U k_{FI}\sin\theta_{I1}. \end{aligned} \tag{23}$$

Using the BTK formalism, the normalized differential tunneling conductance at zero temperature is given by,

$$G(E) = \frac{G_S(E)}{G_N} \tag{24}$$

where the numerator in RHS is given by,

$$G_S(E) = \sum_\sigma \int_{-\pi/2}^{\pi/2} d\theta_{N1}\cos\theta_{N1} G_\sigma(E,\theta_{N1}). \tag{25}$$

In the above expression, the angle and spin resolved conductance, $G_\sigma(E,\theta_{N1})$ is given by,

$$G_\sigma(E,\theta_{N1}) = 1 + |a_\sigma(E,\theta_{N1})|^2\frac{k_{N2}}{k_{N1}} - |b_\sigma(E,\theta_{N1})|^2 \tag{26}$$

and G_N is the conductance for a metal–metal–metal junction.

To make lucid connection to experiments, where disorder effects (although small in cleaner samples) are imperative, we have incorporated the effect of finite quasiparticle lifetimes in all our calculations. In order to consider the shortening of finite quasiparticle lifetime due to the inelastic scattering in the superconductor near the interface, one can introduce [31] a Γ factor into the Bogoliubov equations which renormalizes the quasiparticle energies, E by $E \pm i\Gamma$ and it is defined by, $\Gamma = \frac{1}{\tau_{QP}}$ where τ_{QP} is the finite quasiparticle lifetime. Recently it was shown the conductivity data of disordered MoC superconducting films [32] can only be satisfactorily explained by invoking a finite quasiparticle lifetime. A reasonable estimate of Γ yields $\Gamma/\Delta_0 = 0.05$.

Before we embark into discussing our results, let us include a note on the values of the parameters used in our numerical computation. The Fermi energy of the metallic region has been taken to be 150 times the superconducting gap, that is, $E_F^N = 150\Delta$. The strength of the RSOC term is considered to have representative values of $U = 1$ and $U = 3$ which represent small and intermediate values respectively. We have checked with smaller and larger values of the RSOC parameters in addition to the ones considered here, however there have similar ramifications on the results discussed here. The Rashba free case is included for comparison. It may be noted that the strength of Rashba coupling has the dimension of energy scaled by the Fermi wavevector, which is rendered dimensionless.[1] Lastly, the potential mismatch of the superconducting region with respect to that of the metallic electrode is taken as, $V_1 = 10^3 E_F^N$ [33], implying a large shift of the superconducting Fermi energy compared to the normal state Fermi energy and thus should be a reasonable assumption.

3 Interplay of RSOC and effective barrier potential

3.1 *s*-wave superconductor

We begin with the results for a *s*-wave superconductor. We introduce a dimensionless effective barrier potential $\chi = k_F^I d$ where k_F^I is the Fermi wave vector and d is the barrier width of the insulating region. The Fermi wave vector of the insulating region is proportional to the barrier potential, V_0 (see Eq. (5)). As we shall see, this effective barrier potential, $\chi \sim \sqrt{V_0}d$ is going to play a key role in the subsequent analysis.

In Figure 2, the tunneling conductance, G is shown as function of χ for a *s*-wave superconductor as the RSOC strength is tuned. We can see that the tunneling conductance oscillates as the effective barrier potential increases. These oscillations in conductance profile correspond to Fabry Perot-like oscillations observed in various junction devices [34,35]. In fact the oscillation frequency of the conductance profile depends on the parameters of the insulating region lying between the metallic and the superconducting leads.

Moreover, the RSOC term has an interesting effect on the conductance profile. Figure 2 reveals that the tunneling conductance is highly sensitive to RSOC when χ is odd multiples of a quantity η, that is $\chi = (2p+1)\eta$ $(p = 0, 1, 2, 3, \ldots)$ where η has a value, nearly 1.59 in units of $k_F^I d$ (marked as A in Fig. 2), and zero (hence negligibly sensitive) (marked as B in Fig. 2) when χ is nearly even multiples of η. There is another region (marked as C in Fig. 2) where χ is neither even, nor odd multiple of η, which we denote by $\chi \sim (4p+1)\eta/2$. This region is of the importance to us as the conductance enhances as the

[1] Dimension of RSOC, $[U] = [E]/[k_F] = \frac{\hbar[\nu]\lambda}{2\pi} = \frac{\hbar c[\lambda]}{[\lambda]} = 1$ (with $\hbar = c = 1$).

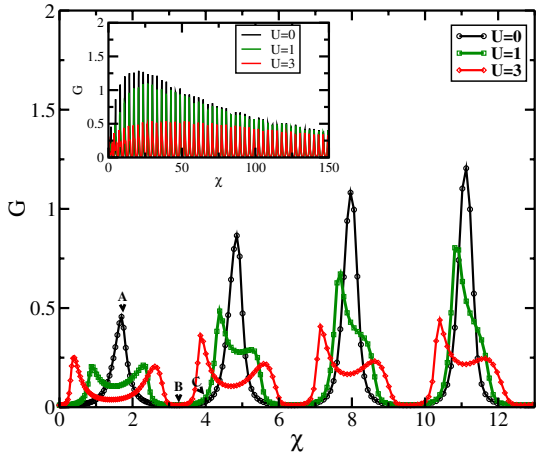

Fig. 2. Black line with circle denotes conductance for $U = 0.0$, the green line with square denotes conductance for $U = 1.0$, the red line with diamond denotes conductance for $U = 3$. Same color coding is followed in subsequent plots. The variation of the conductance, G for a s-wave superconductor as a function of χ ($k_F^I d$) for different strengths of RSOC. The other parameters are $U = 1000E_F^N$, $E/\Delta_0 = 0.0$, $\Gamma/\Delta_0 = 0.05$. The values of U and Γ/Δ_0 are used for the rest of the paper.

strength of RSOC is made larger. For some values of χ, the value of conductance increases with RSOC and at other values it decreases. RSOC broadens the conductance peak and the peak value diminishes. Further with the inclusion of the RSOC term, there is emergence of cusps instead of peaks. From inset of Figure 2 it is clear that for lower values of RSOC, initially the peak value of the G, that is $G_{\max}$ increases with the increasing effective barrier potential, but then it starts to decrease. But for higher values of RSOC, the $G_{\max}$ initially increases but then it remains almost constant. Also it is found that the for higher values of effective potential, χ the effects of RSOC is very minimal.

Let us see how realistic are our predictions made on the conductance oscillation. We shall take typical numbers to test predicted periodicity corresponding to junction parameters that are similar in magnitude with the experiments. For a typical Fermi energy, E_F to have a value of few eV, the Fermi wavevector can be obtained using, $k_F = \sqrt{\frac{2mE_F}{\hbar^2}}$. Taking $E_F = 1\,\text{eV}$ and m same as the bare electronic mass, k_F comes out as $5.14 \times 10^9\,\text{m}^{-1}$. So if the width of the insulating region is few nanometers, then the product of the Fermi wave vector and the width of the insulating region comes out in the order of tens. In our computation, we choose the values of χ as the multiple of η which are order of tens. Thus the parameters for our computation correspond to experimentally relevant parameters.

Now we show the tunneling conductance as the function of biasing energies (scaled by the superconducting gap), for different values of RSOC for χ to be an odd multiple of η, and not an odd multiple of η in Figures 3a and 3b respectively. Specifically we focus on $\chi = 5\eta$ (that is, $p = 2$ for region A) and $5\eta/2$ (that is, $p = 1$ for region C) corresponding to the above cases respectively. There is no particular reason for choosing different values for p, however features are distinct in these region as seen from Figure 2. These values of χ show contrasting features, that is, decreases with RSOC for one ($\chi = 5\eta$) and increases for the other ($\chi = 5\eta/2$). Thus it is clear that the magnitude of the effective barrier potential will decide whether RSOC will enhance or decrease the value of the conductance through a MIS junction.

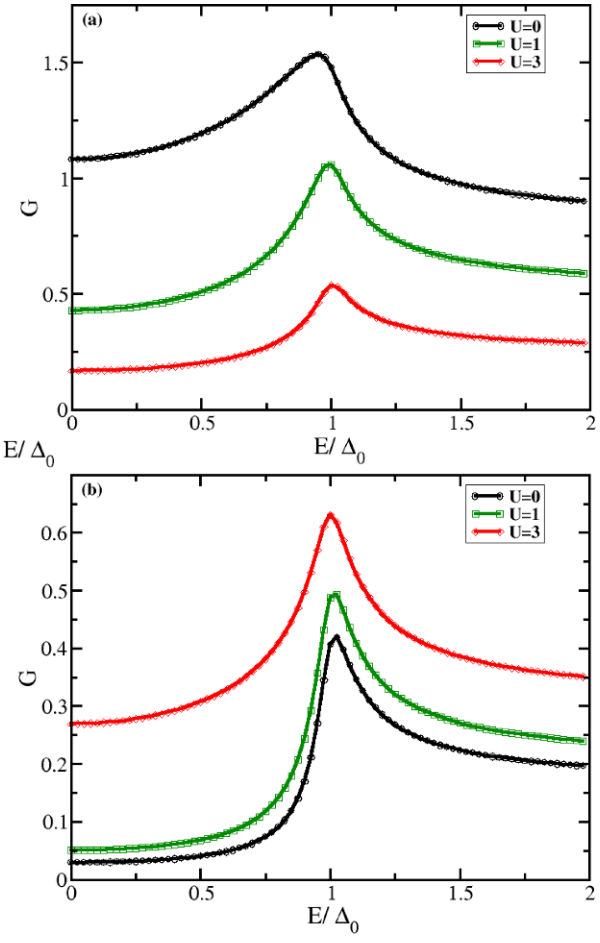

Fig. 3. The variation of the conductance, G for a s-wave superconductor as a function of E/Δ_0 for different strengths of RSOC for (a) $\chi = 5\eta$ and (b) $\chi = 5\eta/2$.

Hence we show the variation of the tunneling conductance, G as a function of Rashba strength, U for different values of χ in Figures 4a and 4b which correspond to $\chi = (2p+1)\eta$ and $\chi = (4p+1)\frac{\eta}{2}$. The features reveal that when the effective barrier potential is nearly an odd multiple of η, the RSOC diminishes the tunneling conductance and the peak height increases with increasing value of p. But after a certain value of p, the peak height decreases which is clear from the inset of Figure 2. From Figure 4b, it is clear that when the effective barrier strength, $\chi \sim (4p+1)\frac{\eta}{2}$, the tunneling conductance initially increases with the RSOC strength but afterwards it decreases with RSOC. So the dependency of the tunneling conductance on the RSOC strength is crucially dependent on the effective barrier potential.

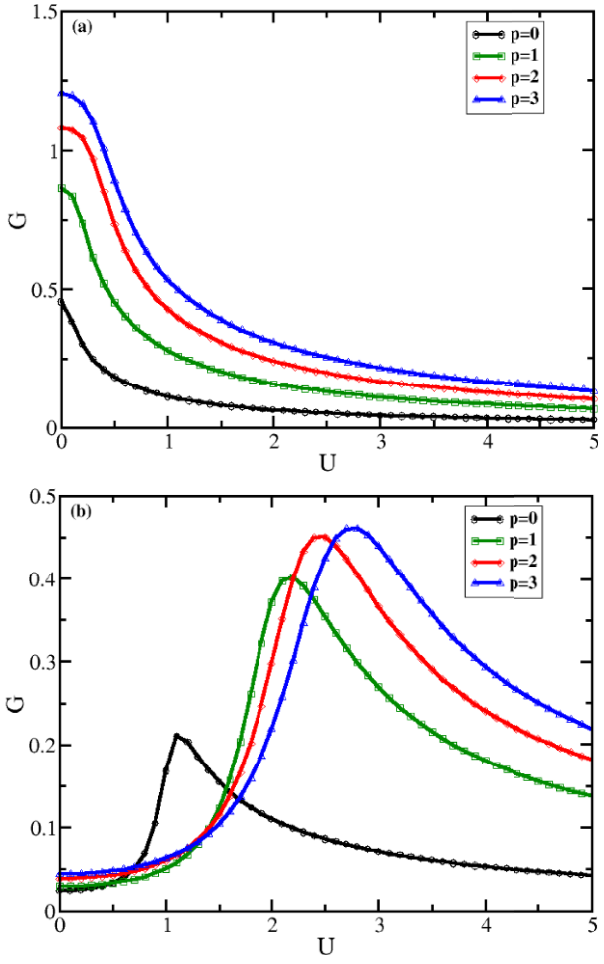

Fig. 4. The variation of the conductance, G for a s-wave superconductor as a function of Rashba strength, U with $E/\Delta_0 = 0$ for (a) $\chi = (2p+1)\eta$ and (b) $\chi = (4p+1)\frac{\eta}{2}$.

Table 1. Behavior of amplitudes of AR and NR with RSOC.

Case	$\chi \sim (2p+1)\eta$	$\chi \sim (4p+1)\eta/2$
AR	Decreases with RSOC	Increases with RSOC
NR	Increases with RSOC	Decreases with RSOC

In equation (26), for the barrier potential to be an odd multiple of η, with increasing RSOC, the contribution of the amplitude AR (the term coming from a_σ) decreases and the amplitude of NR (the term coming from b_σ) increases. But for effective barrier potential where the tunneling conductance increases with RSOC, the reverse happens, that is the amplitude of NR decreases and the amplitude of AR increases. Thus a scrutiny of Figures 4a and 4b yields that the Rashba free case dominates when χ is near an odd multiple of η and for some other values of χ, the RSOC augments the conductance spectrum. These results are summarized in Table 1 where the behavior of amplitudes of AR and NR with RSOC are tabulated.

If we look into the equation (26), it is clear that a larger a_σ enhances G_σ, while a larger b_σ decreases it. So all the

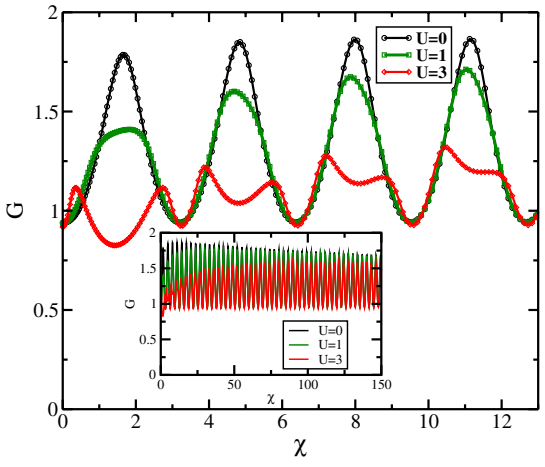

Fig. 5. The variation of the conductance, G for a p-wave superconductor as a function of χ for different strengths of RSOC with $E/\Delta_0 = 0$.

results can be explained from the behavior of AR and NR amplitudes. As we must emphasize that there is no a priori intuition how the interplay of this factor with RSOC in deciding the behavior of conductance.

3.2 Other pairing symmetries

To ascertain whether the superconducting gap function has an additional role to play in the shape and features of the conductance spectrum, and in particular how it interplays with the RSOC, we have considered other pairing symmetries, such as the p-wave and d-wave superconducting correlations. We find that the tunneling conductances as the function of effective barrier potential, χ for a p and d-wave superconductor show similar oscillatory behavior with the same periodicity as observed for a s-wave superconductor. The differences in conductance profiles lie in its values. However there is a significant differences in the features of the conductance spectrum as a function of biasing energies for the p- and d-wave superconductors compared to that of the s-wave superconductor.

3.2.1 p-wave superconductor

We show the tunneling conductance as the function of effective barrier potential, χ for a p-wave superconductor in Figure 5. The comparison between Figure 2 (for the s-wave case) and Figure 5 reveals that the maximum and minimum values of the conductance for a p-wave superconductor is larger than that of a s-wave superconductor. From the inset of Figure 5 it is understandable that for the Rashba free case, the $G_{\max}$ initially increases and then slowly decreases with increasing value of χ. With the inclusion of RSOC, the $G_{\max}$ increases initially, and hence remains almost constant.

Now we study the tunneling conductance as the function of E/Δ_0 for a p-wave superconductor in Figures 6a and 6b for two representative values of χ for which the dependence of conductance spectrum on RSOC

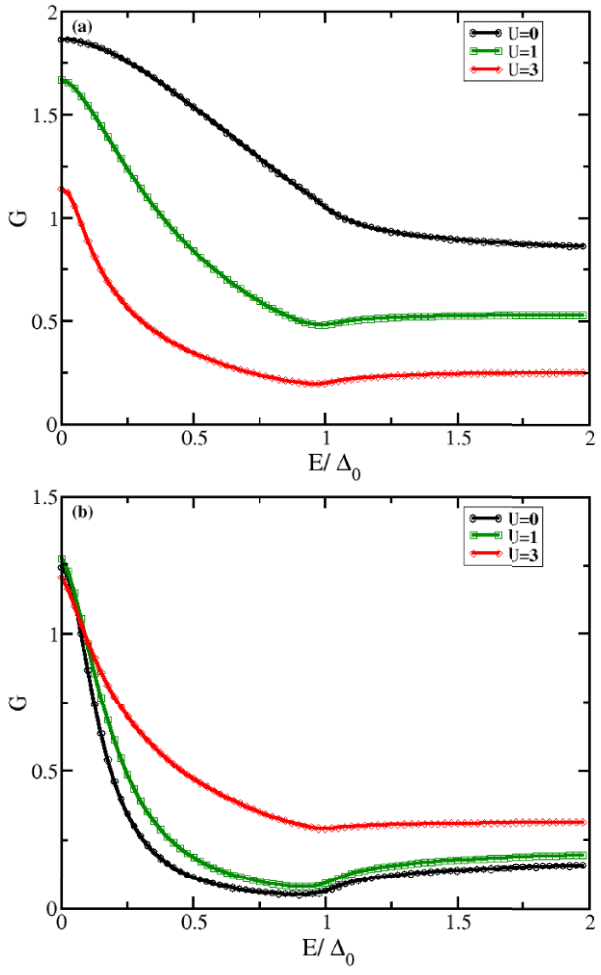

Fig. 6. The variation of the conductance, G for a p-wave superconductor as a function of E/Δ_0 for different strengths of RSOC for (a) $\chi = 5\eta$ and (b) $\chi = 5\eta/2$.

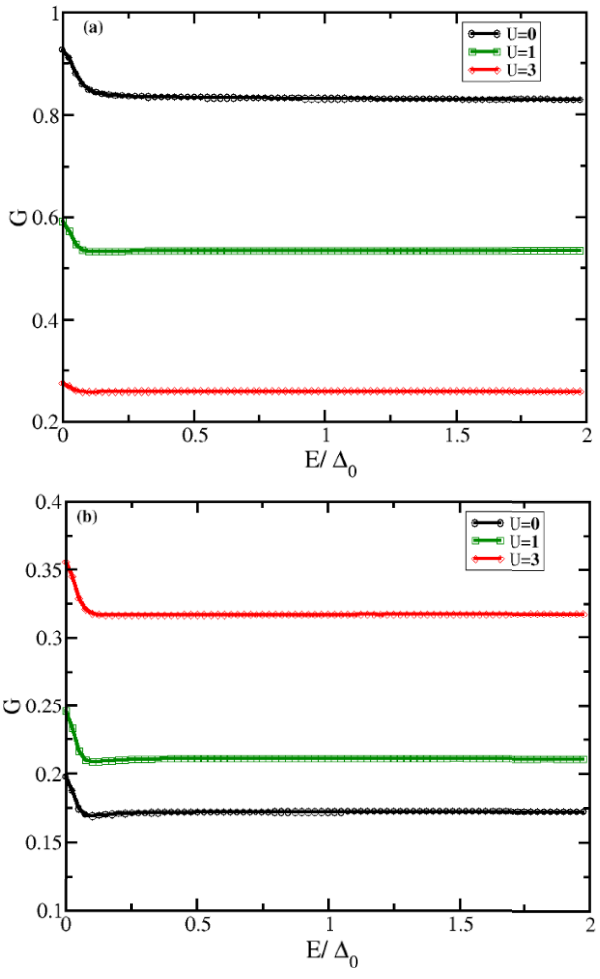

Fig. 8. The variation of the conductance, G for a d-wave superconductor with $\alpha = \pi/4$ as a function of E/Δ_0 for different strengths of RSOC for (a) $\chi = 5\eta$ and (b) $\chi = 5\eta/2$.

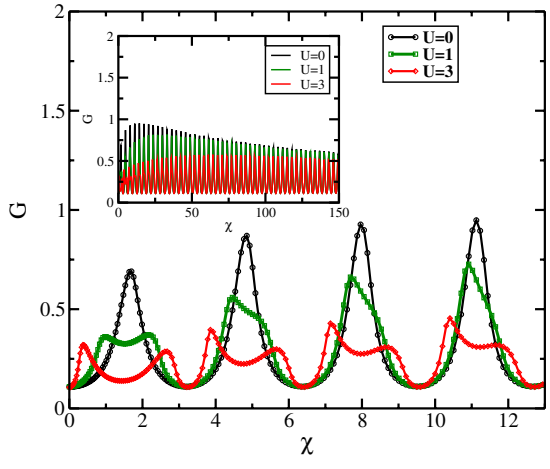

Fig. 7. The variation of the conductance, G for a d-wave superconductor with $\alpha = \pi/4$ as a function of χ for different strengths of RSOC with $E/\Delta_0 = 0.0$.

shows distinct features. Figure 6a shows that with increasing value of RSOC the tunneling conductance decreases, while Figure 6b shows the contradicting character.

3.2.2 d-wave superconductor

It may be noted form equation (7) that the d-wave order parameter can have any arbitrary phase (given by α). For concreteness, one can consider $\alpha = 0, \pi/4$, etc. It is observed that the conductance plots corresponding to $\alpha = 0$ have very similar variation with the biasing energy as that of a s-wave superconductor. Thus they are not repeated here and we only present the plots for $\alpha = \pi/4$.

We present the tunneling conductance as a function of χ for a d-wave superconductor in Figure 7 which shows oscillations with the same periodicity as that for the s-wave and p-wave cases. From Figures 2, 5 and 7 it is easily seen that p wave superconductor shows maximum zero bias ($E/\Delta_0 = 0$) conductance. Figures 8a and 8b denote the tunneling conductances as a function of biasing energy, E/Δ_0 for two distinct values of χ. Figure 8 also reveals the

distinct effect of RSOC on conductance profile for different effective barrier potential.

As said earlier, it can be seen that the conductance profiles as the function of E/Δ_0 for different types of superconducting order parameters are different. The difference is due to the fact that corresponding to different pairing symmetries, the AR becomes maximum and NR becomes minimum at different values of E/Δ_0. But for all superconducting order parameters, the dependence of tunneling conductance on RSOC are almost same.

It is known that the tunneling conductance characteristics for a d-wave case corresponding to $\alpha = \pi/4$ (see Eq. (8)) host a peak at zero energy. It is known as zero bias conductance peak (ZBCP) which is a signature of zero energy surface Andreev boundstate (SABS) [28,36–38]. However in our case the peak, although can be cursorily seen at $E = 0$, is severely suppressed due to the inclusion of the finite quasiparticle lifetime (τ) and a finite width of the insulating region (d). In this limit of $\tau \to 0$ and $d \to 0$, the sharp divergence at $E = 0$ can be recovered.

4 Conclusions

We have investigated the tunneling conductance of a device consisting of a MIS junction where the insulating layer is defined by a barrier width, d and a barrier potential, V_0 with RSOC being present at the interfaces of the system. The key results can be highlighted as follows. We observe an oscillatory behavior for the tunneling conductance spectrum as a function of the effective barrier potential (containing both V_0 and d). The spin–orbit term shows interesting interplay with the effective barrier potential, in the sense that the conductance is highly sensitive to RSOC for certain ranges of this potential; while for others it is nearly insensitive. In particular, the sensitivity is larger when the periodicity is odd multiples of a certain value of this effective potential, while it is less sensitive when the above condition is violated. This periodicity has also a role to play in the profile of the tunneling conductance as a function of the biasing energy. Further, larger values of RSOC have a destructive effect on the conductance when the periodicity satisfies the odd multiple condition, while it has just the reverse trend when the periodicity is not an odd multiple. These results are shown to have a simple explanation in terms of amplitudes of the normal and Andreev reflections. Qualitatively similar features persist for the oscillation profile corresponding to other superconducting pairing gaps, such as p and d-wave symmetries. Although the conductance as a function of the biasing energy shows different behavior, in the sense that the conductance peaks occur at different energies for different pairing symmetries.

As stated earlier, the strength of RSOC can be tuned using an external gate voltage. Hence our studies on the conductance spectrum have the prospects of being important inputs to experimental studies which aim to achieve desired conductance of a MIS junction device. Desired current can be attained with precision by tuning the RSOC strength to an appropriate value as pointed out by our work.

SB thanks SERB, India for financial support under the Grant F. No: EMR/2015/001039.

Author contribution statement

Both the authors have contributed equally on the contents of the paper.

References

1. G. Deutscher, Rev. Mod. Phys. **77**, 109 (2005)
2. D. Daghero, R.S. Gonnelli, Supercond. Sci. Technol. **23**, 043001 (2010)
3. A.F. Andreev, T.M. Rice, Sov. Phys. JETP **19**, 1228 (1964)
4. A.F. Andreev, Zh. Eksp. Teor. Fiz. **46**, 1823 (1964)
5. A. Furusaki, M. Tsukada, Solid State Commun. **78**, 299 (1991)
6. G.A. Prinz, Science **282**, 1660 (1998)
7. I. Zutic, J. Fabian, S. Das Sarma, Rev. Mod. Phys. **76**, 323 (2004)
8. D. Awschalom, D. Loss, N. Samarth, *Semiconductor spintronics and quantum computation* (Springer, Berlin, 2002)
9. T. Matsuyama, R. Kirsten, C. Meiniser, U. Merkt, Phys. Rev. B **61**, 15588 (2000)
10. E.I. Rashba, Fiz. Tverd. Tela (Leningrad) **2**, 1224 (1960)
11. J. Nitta, T. Akazaki, H. Takayanagi, T. Enoki, Phys. Rev. Lett. **78**, 1335 (1997)
12. M.I. Dyakonov, V.I. Perel, JETP Lett. **13**, 467 (1971)
13. J.E. Hirsch, Phys. Rev. Lett. **83**, 1834 (1999)
14. S. Murakami, N. Nagaosa, S.-C. Zhang, Science **301**, 1348 (2003)
15. S. Murakami, N. Nagaosa, S.-C. Zhang, Phys. Rev. B **69**, 235206 (2004)
16. J. Sinova, D. Culcer, Q. Niu, N.A. Sinitsyn, T. Jungwirth, A.H. MacDonald, Phys. Rev. Lett. **92**, 126603 (2004)
17. Y.K. Kato, R.C. Myers, A.C. Gossard, D.D. Awschalom, Science **306**, 1910 (2004)
18. J. Wunderlich, B. Kaestner, J. Sinova, T. Jungwirth, Phys. Rev. Lett. **94**, 047204 (2005)
19. L. Sheng, D.N. Sheng, C.S. Ting, Phys. Rev. Lett. **94**, 016602 (2005)
20. B.K. Nikolic, S. Souma, L.P. Zarbo, J. Sinova, Phys. Rev. Lett. **95**, 046601 (2005)
21. S.-Q. Shen, Phys. Rev. Lett. **95**, 187203 (2005)
22. S. Souma, B.K. Nikolic, Phys. Rev. Lett. **94**, 106602 (2005)
23. S. Wu, K.V. Samokhin, Phys. Rev. B **81**, 214506 (2010)
24. S. Wu, K.V. Samokhin, Phys. Rev. B **82**, 184501 (2010)
25. X. Li, Physica C **485**, 35 (2013)
26. G.E. Blonder, M. Tinkham, T.M. Klapwijk, Phys. Rev. B **25**, 4515 (1982)
27. P.G. de Gennes, *Superconductivity of metals and alloys* (Westview Press, Oxford, 1999)
28. Y. Tanaka, S. Kashiwaya, Phys. Rev. Lett. **74**, 3451 (1995)
29. S. Kashiwaya, Y. Tanaka, Phys. Rev. B **53**, 2667 (1996)
30. P. Kapri, S. Basu, Eur. Phys. J. B **90**, 33 (2017)

31. A. Plecenik, M. Grajcar, S. Benacka, P. Seidel, A. Pfuch, Phys. Rev. B **49**, 10016 (1994)
32. M. Zemlicka, P. Neilinger, M. Trgala, M. Rehak, D. Manca, M. Grajcar, Phys. Rev. B **92**, 224506 (2015)
33. R. Vali, M. Vali, J. Phys.: Condens. Matter **24**, 325702 2012)
34. Y. Zhang, M. Han, L. Shen, Physica B **405**, 1168 (2010)
35. A.V. Kretinin, R.P. Biro, D. Mahalu, H. Shtrikman, Nano Lett. **10**, 3439 (2010)
36. M. Covington, M. Aprili, E. Paraoanu, L.H. Greene, F. Xu, J. Zhu, C.A. Mirkin, Phys. Rev. Lett. **79**, 277 (1997)
37. J.Y.T. Wei, N.C. Yeh, D.F. Garrigus, M. Strasik, Phys. Rev. Lett. **81**, 2542 (1998)
38. S. Kashiwaya, Y. Tanaka, Phys. Rev. B **51**, 1350 (1995)